Available online at www.sciencedirect.com
ScienceDirect
Journal of Solid State Chemistry 181 (2008) 355–364
JOURNAL OF SOLID STATE CHEMISTRY
www.elsevier.com/locate/jssc

High-pressure X-ray diffraction study of $SrMoO_4$ and pressure-induced structural changes

Daniel Errandonea[a,*], Ravhi S. Kumar[b], Xinghua Ma[c,d], Chaoyang Tu[c,d]

[a]*MALTA Consolider Team—Departamento de Física Aplicada-ICMUV, Universitat de València, Edificio de Investigación, c/Dr. Moliner 50, 46100 Burjassot, Valencia, Spain*
[b]*Department of Physics and Astronomy, High Pressure Science and Engineering Center, University of Nevada, 4505 Maryland Parkway, Las Vegas, NV 89154-4002, USA*
[c]*Fujian Institute of Research on the Structure of Matter, Chinese Academy of Sciences, Fuzhou, Fujian 350002, China*
[d]*Graduated School of Chinese Academy of Science, 100039 Beijing, China*

Received 8 October 2007; received in revised form 5 December 2007; accepted 9 December 2007
Available online 23 December 2007

Abstract

$SrMoO_4$ was studied under compression up to 25 GPa by angle-dispersive X-ray diffraction. A phase transition was observed from the scheelite-structured ambient phase (space group $I4_1/a$) to a monoclinic fergusonite phase (space group $I2/a$) at 12.2(9) GPa. The unit-cell parameters of the high-pressure phase are $a = 5.265(9)$ Å, $b = 11.191(9)$ Å, $c = 5.195\ (5)$ Å, and $\beta = 90.9(1)^\circ$, $Z = 4$ at 13.1 GPa. There is no significant volume collapse at the phase transition. No additional phase transitions were observed and on release of pressure the initial phase is recovered, implying that the observed structural modifications are reversible. The reported transition appeared to be a ferroelastic second-order transformation producing a structure that is a monoclinic distortion of the low-pressure phase and was previously observed in compounds isostructural to $SrMoO_4$. A possible mechanism for the transition is proposed and its character is discussed in terms of the present data and the Landau theory. Finally, the room temperature equation of states is reported and the anisotropic compressibility of the studied crystal is discussed in terms of the compression of the Sr–O and Mo–O bonds.
© 2008 Elsevier Inc. All rights reserved.

PACS: 62.50.+p; 61.50.Ks; 64.70.Kb

Keywords: Scheelite; High pressure; X-ray diffraction; Phase transition; Molybdate; Tungstate; Zircon

1. Introduction

Metal molybdates ($AMoO_4$) and tungstates (AWO_4) of relatively large bivalent cations (ionic radius >0.99 Å; A = Ca, Ba, Sr, Pb or Eu, and Cd only for the molybdates) crystallize in the so-called scheelite structure (scheelite = $CaWO_4$) [1], which belongs to the tetragonal space group (SG) $I4_1/a$. The scheelite structure of strontium molybdate ($SrMoO_4$) is shown in Fig. 1. In this structure, each Mo site is surrounded by four equivalent O sites in approximately tetrahedral symmetry. On the other hand, each Sr site is surrounded by eight O sites forming a bisdisphenoid polyhedron.

Scheelite-structured compounds belonging to the molybdate and tungstate families possess attractive luminescence and interesting structural properties. Because of their physical and chemical properties they are used in several technological applications. In particular, scheelite-type crystals are used as scintillators [2], laser-host materials [3], cryogenic detectors for dark matter [4], or heterogeneous catalysts [5]. Alkaline-earth molybdates form part of these compounds. They produce a green luminescence required for their uses in electro-optical devices [6] and recent studies have shown that these molybdate crystals have good prospects as possible negative electrode materials to replace the graphite presently being used in the Li-ion batteries [7]. Scheelite molybdates and tungstates are also being considered for the development of eye-safe Raman lasers [8]. Understanding the electro-optical and

*Corresponding author. Fax: +34 96 3543146.
E-mail address: daniel.errandonea@uv.es (D. Errandonea).

0022-4596/$ - see front matter © 2008 Elsevier Inc. All rights reserved.
doi:10.1016/j.jssc.2007.12.010

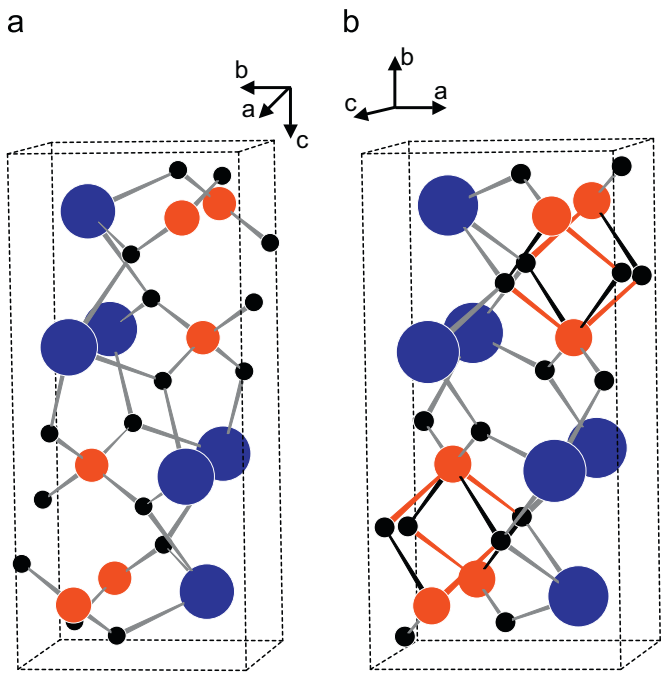

Fig. 1. (color online) (a) The scheelite structure of $SrMoO_4$ at 0.5 GPa and (b) the fergusonite structure of $SrMoO_4$ at 24 GPa. Large blue circles represent the Sr atoms, middle-size red circles the Mo atoms and small black circles the O atoms. The unit cell, Sr–O bonds, and Mo–O bonds are also shown. In (b), we also illustrate that at high pressure the Mo coordination changes from 4 to 6 with two short bonds (gray), two middle-size bonds (red), and two large bonds (black); see text and Fig. 6.

structural properties of these compounds is very important for the above-mentioned applications.

High-pressure research has proven to be an efficient tool to improve the understanding of the main physical properties of AWO_4 and $AMoO_4$ compounds. However, most of the previous studies have been performed on scheelite-type tungstates [9–20], having been established that they undergo a sequence of high-pressure phase transformations with space-group changes $I4_1/a \rightarrow I2/a \rightarrow P2_1/n$. In addition, optical-absorption measurements [21] and luminescence studies [22] have shown that the electronic structure of scheelite tungstates is also strongly affected by pressure. In contrast to the tungstates, there are many open questions regarding the high-pressure structural behavior of the molybdates. They have been studied under compression using Raman spectroscopy [23–27]. In these studies, evidence of structural changes has been reported at pressures ranging from 5 to 12 GPa. Further, in $BaMoO_4$ and $CdMoO_4$ evidence of a second phase transition was found at 9 and 25 GPa, respectively. High-pressure crystallographic studies have been performed on $CaMoO_4$ and $BaMoO_4$ up to about 15 GPa [28,29]. These studies have shown that the high-pressure phases of $CaMoO_4$ and $BaMoO_4$ have a monoclinic fergusonite-type structure (SG: $I2/a$), resembling the high-pressure behavior of the isomorphic tungstates [11,12,15]. On the contrary, previous X-ray diffraction studies on $CdMoO_4$ [30] suggested that the first pressure-driven phase transition is from the tetragonal $I4_1/a$ space group to the monoclinic $P2/c$ space group. On the other hand, contrasting with $BaMoO_4$ and $CdMoO_4$, Raman measurements performed on $SrMoO_4$ to pressures up to 37 GPa [25] only found a phase transition around 12–15 GPa. However, *ab initio* calculations predicted that more than one phase transition should take place in this pressure range [31]. These calculations also suggested that the post-scheelite phase of $SrMoO_4$ is monoclinic but belongs to the space group $P2_1/n$. All these facts show that despite the experimental and theoretical efforts made in the past, we have not yet achieved a full understanding of the high-pressure structural behavior of scheelite-type molybdates.

The aim of the present study is to examine comprehensively the crystal stability of $SrMoO_4$ up to 25 GPa. In order to improve the current understanding of the structural behavior of scheelite-type $AMoO_4$ compounds we have performed angle-dispersive X-ray powder diffraction (ADXRD) measurements in a diamond-anvil cell (DAC) at room temperature (RT). From our experiments, we found that strontium molybdate undergoes a scheelite-to-fergusonite phase transition at 12.2(9) GPa which is reversible. No other structural change was detected up to 25 GPa. In addition to that, based upon our experimental results and the Landau theory, we concluded that the reported phase transition is a second-order ferroelastic transformation. The reported results may be relevant for a better understanding of the structural behavior not only of scheelite-structured molybdates, but also of vanadates, germanates, and silicates.

2. Experimental details

The samples used in our experiments were pre-pressed pellets prepared using a finely ground powder obtained from a single crystal of $SrMoO_4$. This single crystal was grown at the Fujian Institute of Research by the Czochralski method [32]. The as-grown crystal was optically transparent and color free. Before loading the samples into the DAC, their phase purity was tested with a laboratory X-ray diffractometer operated with Cu–$K\alpha$ radiation. The diffraction lines for $SrMoO_4$ collected at ambient pressure (0.0001 GPa) showed only a single scheelite phase with unit-cell parameters $a = 5.394(5)$ Å and $c = 12.019(9)$ Å, in agreement with reported literature values [33].

$SrMoO_4$ powder samples were loaded in a 130 μm hole of a rhenium gasket in a Mao–Bell-type DAC with diamond-culet sizes of 350 μm. A few ruby grains were also loaded with the sample for pressure determination [34] and silicone oil was used as pressure-transmitting medium [35,36]. ADXRD experiments were carried out at Sector 16-IDB of the HPCAT, at the Advanced Photon Source (APS), with an incident wavelength of 0.41514 Å. The monochromatic X-ray beam was focused down to $10 \times 10\,\mu m^2$ using Kickpatrick–Baez mirrors. The images were collected using a MAR345 image plate located

350 mm away from the sample and then integrated and corrected for distortions using FIT2D [37]. The structure solution, and refinements were performed using the POWDERCELL [38] program package.

3. Results and discussion

3.1. Low-pressure phase

The *in situ* ADXRD data measured at different pressures are shown in Fig. 2. The X-ray patterns could be indexed with the scheelite structure (stable at normal conditions) up to 11.3 GPa. In Fig. 3, we show X-ray diffraction patterns of $SrMoO_4$ measured at 0.5 and 11.3 GPa. The spectra are plotted together with the refined structure model and the refinement residuals with the aim of illustrating the quality of the structural refinements used to extract the lattice parameters and bond lengths presented in this work. The full Rietveld refinement of the profile measured at 0.5 GPa with the scheelite model converged to small *R*-factors: $R_{WP} = 1.65\%$, $R_P = 1.2\%$, and $R(F^2) = 1.45\%$ (116 reflections). In the profile measured at 11.3 GPa the *R*-factors were $R_{WP} = 1.85\%$, $R_P = 1.35\%$, and $R(F^2) = 1.6\%$ (92 reflections). The starting model for the refinement was taken from the previously reported crystal structure of $SrMoO_4$ [33]. Table 1 summarizes the lattice parameters and atomic positions obtained for $SrMoO_4$ at 0.5 and 11.3 GPa. For every data point analyzed up to 11.3 GPa, we found a good agreement between the refined profiles and the experimental diffraction patterns. We also observed that the atomic positions remain nearly unchanged from ambient pressure to 11.3 GPa within the accuracy of the refinements (see Table 1).

Splitting and broadening of the diffraction peaks were observed at 13.1 GPa together with the appearance of new reflections. In particular, the strongest intense peak of

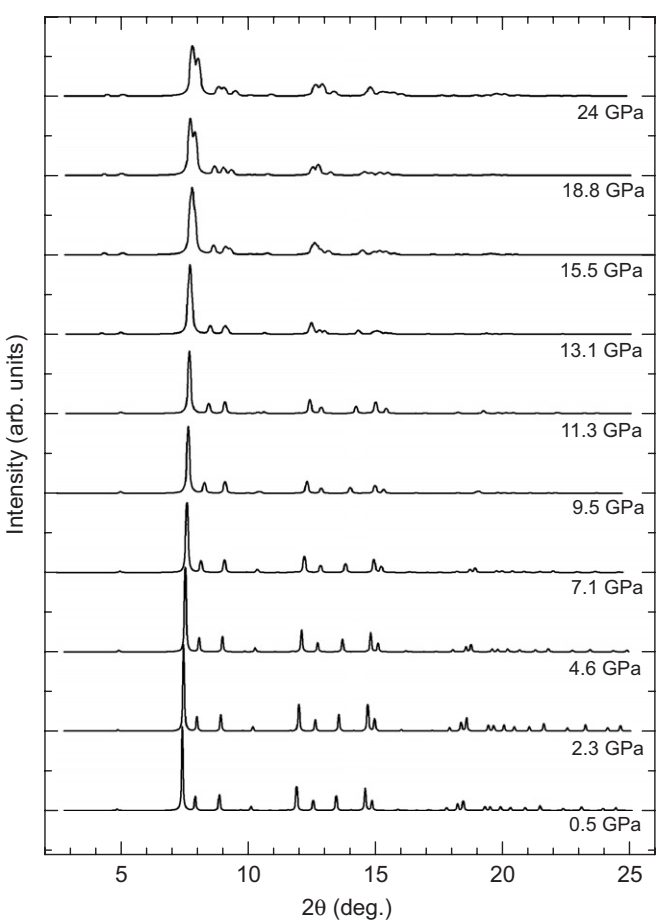

Fig. 2. Room-temperature ADXRD data of $SrMoO_4$ at different pressures up to 24 GPa. In all diagrams, the background was subtracted. Pressures are indicated in the plot.

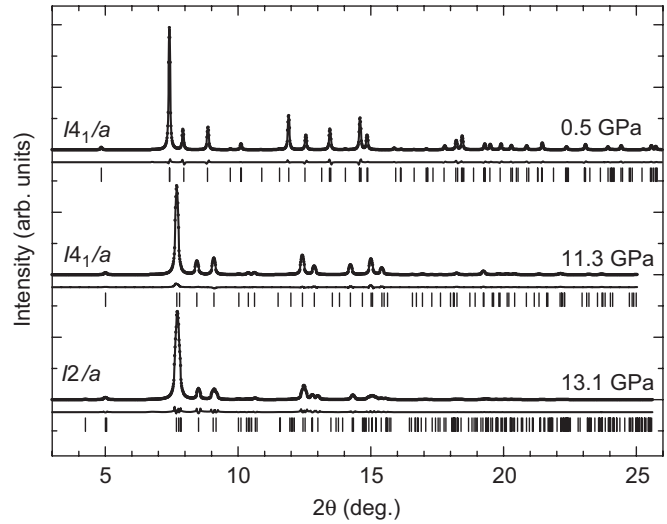

Fig. 3. ADXRD patterns of $SrMoO_4$ at 0.5, 11.3, and 13.1 GPa. The background was subtracted. The dots are the experimental data and the solid lines the refined profiles. The difference between the measured data and the refined profiles is also represented. The bars indicate the calculated positions of the reflections.

Table 1
Structural parameters of the scheelite and fergusonite structure of $SrMoO_4$

	Site	*x*	*y*	*z*
(a) *Structural parameters of scheelite $SrMoO_4$ at 0.5 GPa: $I4_1/a$, $Z = 4$, $a = 5.380(5)$ Å, $c = 12.019(9)$ Å*				
Sr	4*b*	0	0.25	0.625
Mo	4*a*	0	0.25	0.125
O	16*f*	0.248(9)	0.110(6)	0.051(6)
(b) *Structural parameters of scheelite $SrMoO_4$ at 11.3 GPa: $I4_1/a$, $Z = 4$, $a = 5.238(5)$ Å, $c = 11.272(9)$ Å*				
Sr	4*b*	0	0.25	0.625
Mo	4*a*	0	0.25	0.125
O	16*f*	0.247(9)	0.119(6)	0.050(6)
(c) *Structural parameters of fergusonite $SrMoO_4$ at 13.1 GPa: $I2/a$, $Z = 4$, $a = 5.256(5)$ Å, $b = 11.191(9)$ Å, $c = 5.195(5)$ Å, $\beta = 90.9(1)°$*				
Sr	4*e*	0.25	0.615(2)	0
Mo	4*e*	0.25	0.123(1)	0
O	8*f*	0.910(6)	0.951(6)	0.248(5)
O	8*f*	0.492(6)	0.239(5)	0.797(6)

These parameters were obtained from the present Rietveld refinements (see text).

scheelite, the (112) reflection, observed around $2\theta = 7.7^\circ$ at 11.3 GPa split into two peaks. The same fact occurs with the (200) and (204) reflections located at 11.3 GPa around $2\theta = 9.1^\circ$ and 12.4°, respectively. In addition to that, at 13.1 GPa new weak peaks can be clearly observed in Fig. 2 at $2\theta = 4.2^\circ$ and 12.8°. These changes in the diffraction patterns indicated a structural phase transition. In order to estimate the transition pressure we take the average of the highest pressure where the diffraction pattern can be assigned to the low-pressure phase (11.3 GPa) and the lowest pressure corresponding to the high-pressure phase (13.1 GPa). The obtained value of 12.2(9) GPa is in agreement with previous Raman observations [25] and with the transition pressure estimated from the MoO_4/Sr radii ratio [39]. The uncertainty of this value is larger than the pressure gradients measured in the pressure chamber during the experiments.

It is important to note here, that looking closely to the diffraction patterns of Fig. 2, it can be seen that the peak at $2\theta = 10.2^\circ$ starts to split at 9.5 GPa. This splitting occurs together with a slight broadening of some of the major peaks. As we will show latter, these changes are related to the anisotropic compressibility of $SrMoO_4$. However, it cannot be discarded that they may originate due to a phase coexistence of the low- and high-pressure phases as already observed in Raman experiments on $BaWO_4$ and $PbWO_4$ [9,10].

From the refinement of the X-ray diffraction patterns measured up to 11.3 GPa, we extracted the pressure dependence of the lattice parameters, cell volume, and axial ratios for scheelite $SrMoO_4$. These results are summarized in Figs. 4 and 5. As in other scheelite-structured molybdates [29] and tungstates [11,12,15], the compression of $SrMoO_4$ is highly anisotropic, the c-axis being more compressible than the a-axis. The c/a axial ratio decreases from 2.228 at ambient pressure to 2.152 at 11.3 GPa (see Fig. 4). This anisotropy in the axial compressibility of $SrMoO_4$ is comparable with that of $SrWO_4$ [11]. It should be mentioned that the c/a ratio for $SrMoO_4$ and $SrWO_4$ at ambient pressure is 2.228 and 2.206 [11], respectively. In addition, the unit-cell volumes of the molybdates are generally smaller than those of the tungstate analogs [1], as can be seen by comparing the data shown in Fig. 5 with those published in Ref. [11]. The higher c/a ratio in molybdates can be explained by the higher cation–cation electrostatic repulsion in $SrMoO_4$ than in $SrWO_4$ [12]. The similar change induced by pressure in c/a for both compounds is related to their compressibility which is mainly due to the compression of the SrO_8 dodecahedra as we will show later in this section of the paper. The different compressibility of the c- and a-axis causes the splitting of some X-ray peaks that were degenerated at ambient pressure, being the possible origin of the slight changes observed in the diffraction patterns below the phase-transition pressure.

The pressure–volume curves shown in Fig. 5 were analyzed in the standard way using a third-order Birch–Murnaghan equation of states (EOS) [40]. The bulk modulus (B_0), its pressure derivative (B_0'), and the atomic volume (V_0) at zero pressure obtained for the scheelite

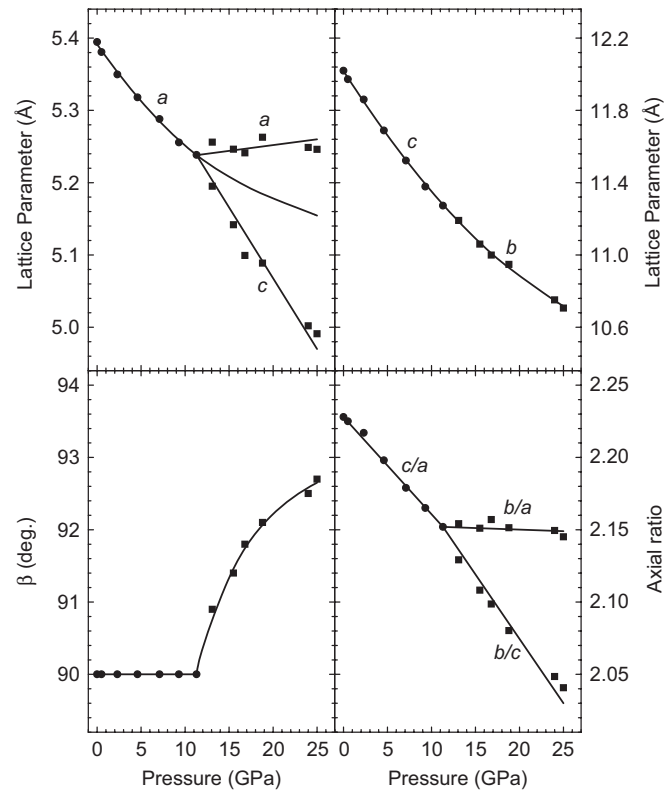

Fig. 4. Evolution of the lattice parameters and axial ratios of $SrMoO_4$ under pressure. Circles: scheelite phase. Squares: fergusonite phase. An extrapolation of the lattice parameters of the low-pressure phase up to 25 GPa is also shown.

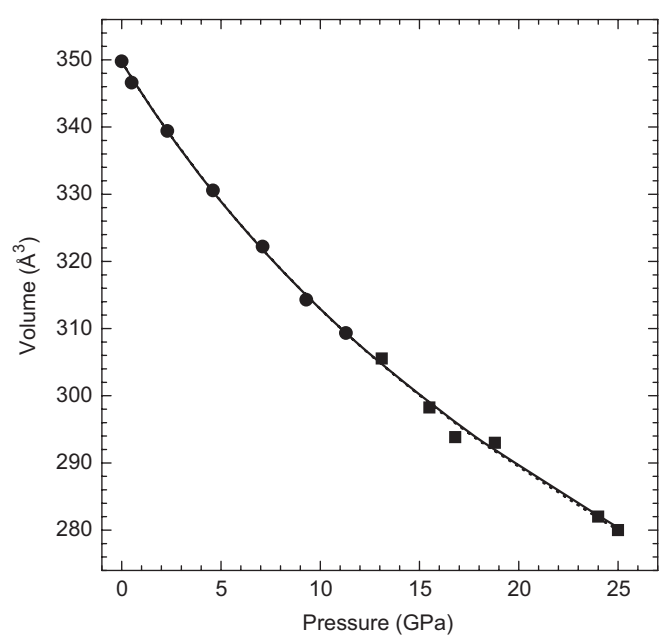

Fig. 5. Volume versus pressure data for scheelite (circles) and fergusonite (squares) $SrMoO_4$. The solid line represents the EOS fitted using only the scheelite data and the dotted line the EOS fitted using all the data. The differences between both EOS can be neglected (see Section 3.2).

phase of $SrMoO_4$ are $B_0 = 71(3)$ GPa, $B_0' = 4.2(4)$, and $V_0 = 349.7(4)$ Å^3. The fitted EOS, shown as a solid line in Fig. 5, matches very well the experimental data. The obtained bulk modulus also agrees with the value calculated from elastic constant data ($B_0 = 74$ GPa) [25]. Previously, it has been empirically determined that the bulk modulus in scheelite-structured ABX_4 compounds is related to the cation charge density of the AX_8 polyhedra [11,41]. In particular, it has been established that B_0 (GPa) $= 610\ Z/d^3$, where Z is the cationic formal charge of A and d is the mean A–X distance at ambient pressure in Å [11]. From our data we obtained a Sr–O distance of 2.578 Å, which agrees within 1% with the value reported by Gurmen [33]. Applying the formula given above, a bulk modulus of 71 GPa is obtained, which agrees with the value obtained from the fitted EOS.

From our experimental data, we have also investigated the evolution of cation–anion distances in $SrMoO_4$. According to our structural refinements, within the pressure stability range of the scheelite structure, the change of the oxygen position coordinates for $SrMoO_4$ under compression is insignificant, being comparable to the experimental errors (see Table 1). This observation is in good agreement with the conclusions drawn from a single-crystal study carried out up to 4.1 GPa by Hazen et al. in other molybdates [41]. Such behavior can be expected for the scheelite-type lattice, as the structure is constructed by hard $(MoO_4)^{2-}$ anions which are surrounded by Sr^{2+} ions to balance the charge. As with increasing of pressure the $(MoO_4)^{2-}$ ions do not show any noticeable changes, also the oxygen positions do not change significantly. Based upon these observations, to calculate the pressure evolution of the cation–anion distances, we assumed the atomic positions obtained at 0.5 GPa (see Table 1) for the whole range of stability of the low-pressure phase. Fig. 6 shows the evolution of the atomic distances between nearest neighbors with increasing pressure. The decrease of Sr–O distances can be compared with the rigidity of the Mo–O bond. In Fig. 6, it can be seen that there are two Sr–O distances, the largest distance being more compressible than the shorter one. We also found that the second neighbors Mo–O distances are more compressible than the first neighbors Mo–O distances. These observations support the description of $AMoO_4$ scheelites in terms of nearly uncompressible anion-like MoO_4 tetrahedra surrounded by charge compensating cations. Upon compression the MoO_4 units remain essentially undistorted and the reduction of the unit-cell size is mainly accounted by the compression of the Sr–O dodecahedral environment. It is important to note that along the a-axis the MoO_4 units are directly aligned, whereas along the c-axis there is a Sr cation between each MoO_4 tetrahedra (see Fig. 1). Therefore, the different arrangement of hard MoO_4 tetrahedra along the c- and a-axis explains the anisotropic axial compressibility of $SrMoO_4$. On the other hand, the fact that the MoO_4 tetrahedra behave basically as uncompressible rigid units in comparison with the SrO_8 polyhedra is

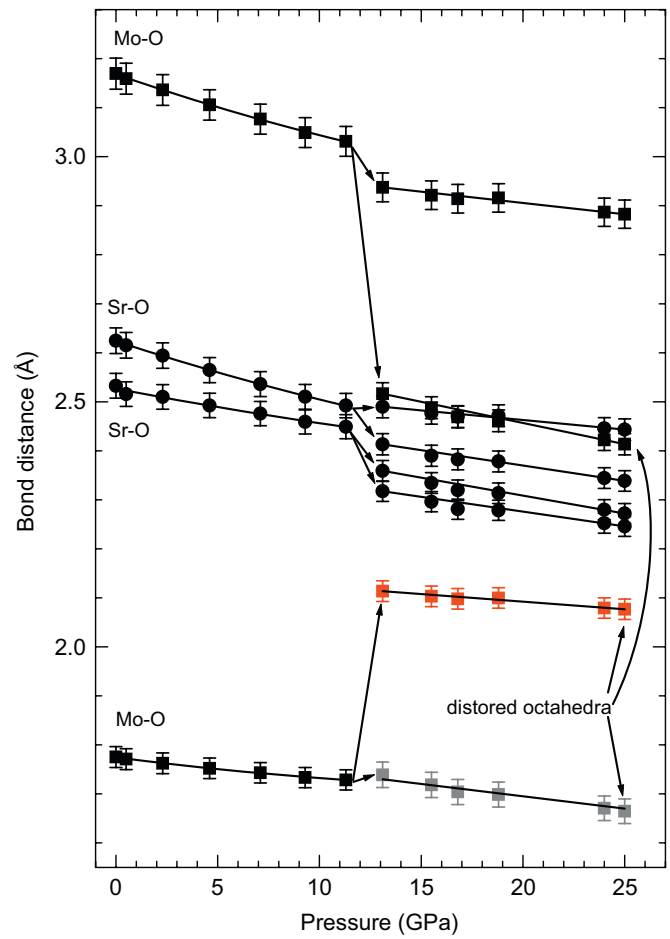

Fig. 6. (Color online) Pressure dependence of the interatomic bond distances in the scheelite and fergusonite phases of $SrMoO_4$. Squares represent the Mo–O distances and circles the Sr–O distances. For the fergusonite phase, the Mo–O bonds that form a distorted octahedral are shown. Short bonds (gray), middle bonds (red), and large bonds (black). The same colors have been used to illustrate the bonds in Fig. 1.

what allows the bulk modulus formula proposed in Ref. [11] to make accurate estimations of B_0 as shown above.

A comparison of the present results obtained for $SrMoO_4$ under high pressure with the reported structural variations at high temperature [42] shows a fairly close but inverse relation with each other. This is illustrated in Fig. 7, where we have plotted the volume dependence of the axial ratio of both compression and thermal expansion. A similar phenomenon was previously documented in $CaMoO_4$ [43]. The high-temperature studies on $SrMoO_4$ and $CaMoO_4$ [42,43] show a systematic increase in c/a with pressure as against the systematic decrease with pressure of the present investigation. In the case of $SrMoO_4$, the change of anisotropy associated with volume shows a similar behavior under compression or expansion. This is also a consequence of the fact that the less rigid (higher ionic) Sr–O bonds have significant expansion or compression compared with the Mo–O bonds. Therefore, the structural evolution under pressure or temperature is basically governed by the SrO_8 polyhedron. The crystal chemistry of $SrMoO_4$ at high temperature shows a similar

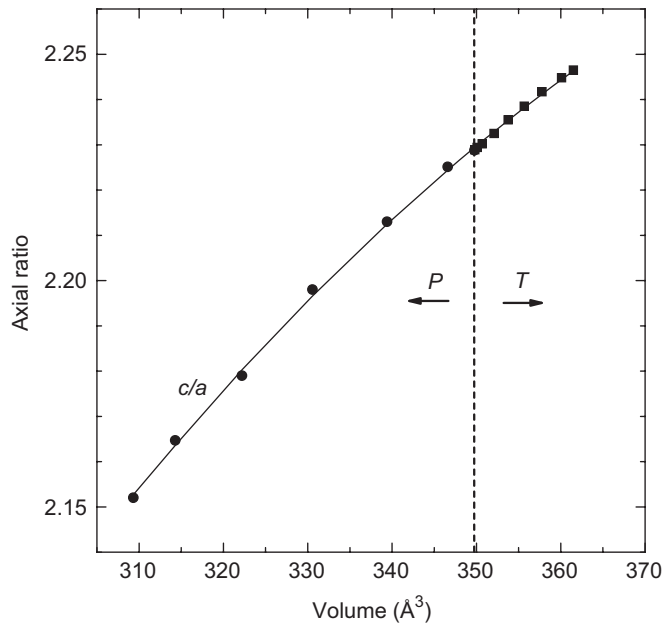

Fig. 7. c/a axial ratio of $SrMoO_4$ as a function of the atomic volume. Circles: present high-pressure data. Squares: data corresponding to the volume expansion observed at high temperature [42]. The solid line is just a guide to the eye. The dashed line delimitates the compression and expansion regions.

linear dependence of the Sr–O bond with pressure or temperature, whereas the Mo–O bonds remain almost invariant in both situations. Thus, we conclude that there is an inverse relationship between pressure and temperature in scheelite-type molybdates, as previously documented for other ABO_4 compounds, like $LaNbO_4$ [44].

3.2. High-pressure phase

As we mentioned above, the ADXRD spectra of $SrMoO_4$ exhibit notorious changes between 11.3 and 13.1 GPa (see Fig. 2). These changes are completely reversible upon pressure release without any significant hysteresis. Beyond 11.3 GPa some of the diffraction peaks split and additional diffraction peaks emerge. In particular, the appearance of new peaks around $2\theta = 4.2^\circ$ and 12.8° can be observed at 13.1 GPa in Fig. 2. The observed splitting of peaks and the appearance of new reflections suggest the occurrence of a pressure-induced phase transition. At pressures higher than 13.1 GPa, some of the broadened diffraction peaks develop into two clearly separated diffraction peaks. In particular, the splitting of the (112) and (200) is easily identifiable in Fig. 2. The measured ADXRD patterns of the high-pressure phase can be indexed on the basis of the monoclinic fergusonite structure (SG: $I2/a$) [45] up to the highest pressure reached in our experiments, discarding the possibility of a second phase transition up to 25 GPa. The observation of a fergusonite-type high-pressure phase is in good agreement with previous studies reported for other alkaline-earth molybdates [28,29]. It is also in good agreement with the systematic of the high-pressure sequence established for ABX_4 compounds using the phase diagram proposed by Bastide [46,47]. This picture for the structural behavior of $SrMoO_4$ is further consistent with the pressure-induced *sp–d* electron transfer in alkaline-earth metals which convert them into an early transition metal-like character [48,49]. Therefore, under compression Sr will take an electron configuration similar to that of Y, and it is known that ABO_4 ternary oxides of Y and transition metals crystallize in the fergusonite structure [50]. In addition, the existence of group–subgroup relationship between the $I4_1/a$ and $I2/a$ space groups makes the reported transition quite reasonable from the crystallochemical point of view [51].

Fig. 3 shows the Rietveld refinements to the experimental spectra of $SrMoO_4$ at 13.1 GPa obtained assuming the fergusonite structure. In order to perform the Rietveld refinement the starting Sr, Mo, and O positions have been derived from the atomic coordinates in the scheelite structure using the $I4_1/a \rightarrow I2/a$ subgroup relationship implemented in the PowderCell program [38]. For all the diffraction patterns measured beyond 11.3 GPa, we obtained good agreement between the fergusonite refined model and the experimental diffraction patterns. The full-profile Rietveld refinement at 13.1 GPa with the fergusonite model converged to small R factors: $R_{WP} = 2.25\%$, $R_P = 1.6\%$, and $R(F^2) = 1.95\%$ (198 reflections). Similar refinement quality was obtained for fergusonite $SrMoO_4$ up to 25 GPa. Table 1 summarizes the lattice parameters and atomic positions obtained for fergusonite $SrMoO_4$. In addition to fergusonite, other structures previously considered as candidates for the high-pressure phases of scheelite-type ABO_4 compounds were considered when analyzing the diffraction patterns of the high-pressure phase. These structures were: $BaWO_4$-II (SG: $P2_1/n$) [52], $HgWO_4$-type (SG: $C2/c$) [53], raspite (SG: $P2_1/a$) [54], wolframite (SG: $P2/c$) [55], α-$MnMoO_4$ ($C2/m$) [17], $LaTaO_4$ (SG: $P2_1/c$) [56], $BaMnF_4$ (SG: $A2_1/am$) [57], $SrUO_4$ (SG: *Pbcm*), [58], *Cmca* (SG: *Cmca*) [11], zircon (SG: $I4_1/amd$) [59], and pseudo-scheelite (SG: *Pnma*) [60]. However, none of these structures can satisfactorily explain the X-ray diffraction patterns collected beyond 11.3 GPa. Therefore, it seems quite reasonable to accept that the high-pressure phase of $SrMoO_4$ has a fergusonite structure. Another fact we would like to emphasize here is that, in our experiments we did not find any diffraction peak that could be assigned to the probable decomposition products of $SrMoO_4$ (i.e. SrO and MoO_3) [61]. This observation and the reversibility of the high-pressure phase to the scheelite phase on release of pressure imply that $SrMoO_4$ like $SrWO_4$ [11] and $BaMoO_4$ [29] does not decompose significantly into the component oxides at high pressures, unlike what was reported in a previous high-pressure study on $SrWO_4$ [62].

Let us comment here again on the peak splitting and broadening observed from 9.5 to 11.3 GPa. We tried to fit the X-ray patterns collected at these pressures with the

fergusonite structure. However, the refinements always lead to a convergence of the fergusonite structure towards the scheelite structure; i.e. the structural parameters of fergusonite take such a values that it reduces to scheelite. We think that this observation is an evidence that the transition pressure is located beyond 11.3 GPa (which is also in good agreement with previous Raman experiments [25]). However, a gradual transformation from scheelite to fergusonite starting at 9.5 GPa should not be completely ruled out. Unfortunately, given the similitude of the fergusonite and scheelite structures, it is very hard to detect such a coexistence in X-ray diffraction experiments. To explore the possible phase coexistence high-pressure Raman experiments will be more convenient.

Fig. 4 shows the lattice parameters of the fergusonite phase of $SrMoO_4$ as a function of pressure up to 25 GPa. Experiments were not extended at higher pressures because the quality of the ADXRD patterns deteriorated above 25 GPa. A similar result was observed previously in $SrWO_4$ [11] and also in other isostructural compounds, being independent of the pressure-transmitting medium employed in the experiments. This may be related to precursor effects either of a martensitic transition [63–65] or of the amorphization observed in alkaline-earth tungstates [16] at higher pressures. Further experiments and theoretical studies will be conducted in the future to clarify this issue. In Fig. 4, it can be seen that after the scheelite-fergusonite phase transition the β angle gradually increases with pressure, changing from 90.9° at 13.1 GPa to 92.7° at 25 GPa. In addition, the difference between the b/a and b/c axial ratios of the fergusonite phase also increases upon compression; see Fig. 4. These two facts imply an increase of the monoclinic distortion with pressure. In Fig. 5, it can be seen that a volume discontinuity is not apparent at the transition pressure, consistent with the fact that fergusonite is a distorted and compressed version of scheelite which only implies a lowering of the point-group symmetry from $4/m$ to $2/m$. A third-order Birch–Murnaghan fit to both the scheelite and the fergusonite pressure–volume data shown in Fig. 5 gives EOS parameters that differ by less than one standard deviation from those obtained for the scheelite data only. Hence, the EOS reported above can be assumed as a valid EOS for $SrMoO_4$ up to 25 GPa, as illustrated in Fig. 5. The differences between the EOS obtained using only the scheelite data (solid line) and using all the data (dotted line) can be neglected.

Now we would like to comment on the changes we observed in the bond distances at the phase transition. In Fig. 6, it can be seen that at the Mo–O bond distances split, becoming the MoO_4 tetrahedra distorted with two short distances (1.739 Å) and two long distances (2.114 Å). In addition to that, the SrO_8 dodecahedra distort in such a way that after the transition there are four different Sr–O distances. In spite of this, in the fergusonite phase, the Sr–O bonds are much more compressible than the Mo–O bonds. As a consequence of it, there are virtually no changes between the bulk compressibility of the two phases of $SrMoO_4$, as the volume versus pressure data of both phases can be represented with the same EOS. Basically, in the high-pressure phase the linear compressibility of the different axis changes due to the monoclinic distortion of the crystal, but the bulk compressibility does not change since it is still governed only by the compression of the SrO_8 dodecahedra. Furthermore, at the phase transition two of the oxygen atoms, which are second neighbors to Mo approach Mo considerably. In addition, this bond distance rapidly decreases with pressure after the phase transition; see Fig. 6. Therefore, the Mo–O coordination gradually changes from 4 to 4 + 2 within the pressure-range of stability of the fergusonite phase. At 25 GPa, there are two short Mo–O bonds of 1.664(25) Å, two medium bonds of 2.077(20) Å, and two large bonds of 2.413(22) Å, which correspond to the bonds shown in Fig. 1(b). The same coordination change has been already observed in $PbWO_4$ [10], where fergusonite acts as a bridge phase between the scheelite phase and a second high-pressure phase with sixfold W–O coordination.

3.3. Structural model for the scheelite-to-fergusonite phase transition

The pressure-driven transition from the tetragonal scheelite to the monoclinic fergusonite phase has been reported to occur not only in other molybdates [11,12,15] and tungstates [28,29] but also it can be temperature-induced in compounds like $LaNbO_4$ around 780 K [44]. There is a evidence that this transition is of second order [66]. This is consistent with viewing the transition as a slight displacement of the atoms, rather than a more dramatic reconstruction of the lattice. As observed in $BaMoO_4$ [29], in $SrMoO_4$ the scheelite-to-fergusonite transition is caused by small displacements of the Sr and Mo atoms from their high-symmetry positions and large changes in the O positions, which consequently lead to a polyhedral distortion (see Fig. 1). In particular, all the Sr and Mo atoms of alternate layers of the scheelite structure shift in opposite directions along the c-axis (b-axis of the fergusonite structure) accompanied by a shear distortion perpendicular to the c-axis of alternate O planes. Because of these atomic displacements, immediately after the transition, the volume of MoO_4 tetrahedra is enlarged by a factor of 10% and the volume of the AO_8 bisdisphenoids is reduced by a similar amount. However, close to the transition pressure, the fergusonite structure still contains isolated MoO_4 tetrahedra interlinked by Sr ions, which have primarily an eightfold O coordination, like in the scheelite structure.

After the phase transition, upon further compression of the fergusonite phase, one pair of parallel unit-cell edges contract, another pair elongates, while the angle between them gradually increases as described above (see Fig. 4). There are two possible ways to achieve this situation and these options can be illustrated by two choices of direction in the tetragonal cell. The two choices are

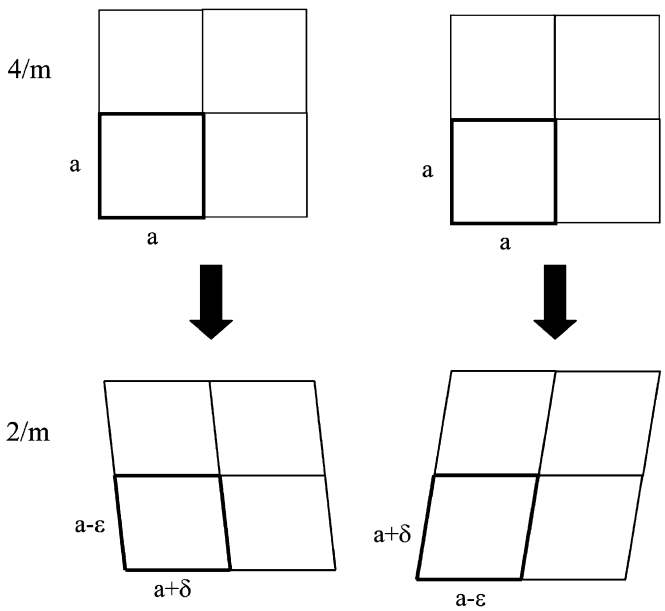

Fig. 8. A schematic view of two orientation states of the plane perpendicular to the c-axis for a scheelite to fergusonite transformation. Because of the fourfold symmetry of the prototypic phase there are two possible ways for the unit cell to deform. ε and δ represent the contraction or expansion of the tetragonal a- and b-axis.

crystallographically identical, and related through the fourfold rotation symmetry of the tetragonal system. In Fig. 8, the transition from the tetragonal system with point group $4/m$ to the monoclinic system with point group $2/m$ is schematically illustrated and the two orientation states for a transformation from scheelite to fergusonite can be visualized. We will call these two monoclinic orientation states S_1 and S_2. They are identical in structure, but different in orientation. These orientation states are crystallographically and energetically equivalent. This makes it impossible to distinguish one from the other if they appear separately. All these facts, strongly suggest that the scheelite to fergusonite transition is not only a second-order transformation but it has also a ferroelastic nature. One possibility to probe this hypothesis is to analyze the spontaneous strains of the monoclinic phase, calculated based upon our X-ray diffraction data, using the Landau theory [67]. This analysis is presented in detail in the next section of the paper.

3.4. Spontaneous strain and the ferroelastic nature of the phase transition

In a ferroelastic transformation, the S_1 and S_2 states can be seen as a small distortion caused by slight displacements of the atoms of the parent phase. The spontaneous strain characterizes the distortion of each orientation state relative to the prototype structure (i.e. the scheelite-type structure). Following Schlenker et al. [68], the elements of the strain tensor for a crystal can be calculated based upon the lattice parameters. In the case of the tetragonal to monoclinic transition of $SrMoO_4$, the elements of one of the orientation states are

$$\varepsilon_{11} = \frac{c_M \sin \beta_M}{a_T} - 1, \tag{1}$$

$$\varepsilon_{22} = \frac{a_M}{a_T} - 1, \tag{2}$$

$$\varepsilon_{33} = \frac{b_M}{c_T} - 1, \tag{3}$$

$$\varepsilon_{12} = \varepsilon_{21} = \frac{1}{2}\frac{c_M \cos \beta_M}{a_T}, \tag{4}$$

where the subscripts T and M refers to the tetragonal and monoclinic phases. The remaining tensor elements are reduced to zero by the cell parameters. The strain tensor for a single orientation state (S_1) is then,

$$e_{ij}(s_1) = \begin{pmatrix} \varepsilon_{11} & \varepsilon_{12} & 0 \\ \varepsilon_{12} & \varepsilon_{22} & 0 \\ 0 & 0 & \varepsilon_{33} \end{pmatrix} \tag{5}$$

and $e_{ij}(S_2)$ is related to $e_{ij}(S_1)$ by $e_{ij}(S_2) = \mathbf{R}\ e_{ij}(S_1)\ \mathbf{R}^T$, where $\mathbf{R}$ and $\mathbf{R}^T$ are the 90° rotation matrix around the b-axis of the monoclinic unit cell and its transpose. According to Aizu [69] in the present case, the spontaneous strain tensor can be expressed as

$$e^s_{ij}(s_1) = e_{ij}(s_1) - \frac{1}{2}\left[e_{ij}(s_1) + e_{ij}(s_2)\right] = \begin{pmatrix} -u & v & 0 \\ v & u & 0 \\ 0 & 0 & 0 \end{pmatrix} \tag{6}$$

and

$$e^s_{ij}(s_2) = \begin{pmatrix} u & -v & 0 \\ -v & -u & 0 \\ 0 & 0 & 0 \end{pmatrix}, \tag{7}$$

where $u = 1/2(\varepsilon_{22} - \varepsilon_{11})$ is the longitudinal spontaneous strain and $v = \varepsilon_{12}$ is the shear spontaneous strain. The scalar spontaneous strain ε_s is defined as [20,66,69]

$$\varepsilon_s^2 = \sum_{i=1}^{3}\sum_{j=1}^{3}(\varepsilon^s_{ij})^2 = 2(u^2 + v^2). \tag{8}$$

Following Eq. (8), we calculated the spontaneous strain tensor as well as the scalar spontaneous strain for $SrMoO_4$ using the lattice-parameter pressure dependences given in Fig. 4. The values of a_T and c_T were extrapolated into the pressure regime of the fergusonite phase ($P > 11.3$ GPa) from its pressure dependence at pressures lower than the transition pressure. These extrapolations are shown in Fig. 4. We have enough experimental data points within the pressure stability range of the scheelite structure for making a good extrapolation. The obtained results are plotted in Fig. 9 as a function of $\sqrt{(P - P_T)/P_T} = \eta'$, where we choose the transition pressure (P_T) as the average of the transition pressure reported here and in Ref. [25], $P_T = 12.65$ GPa.

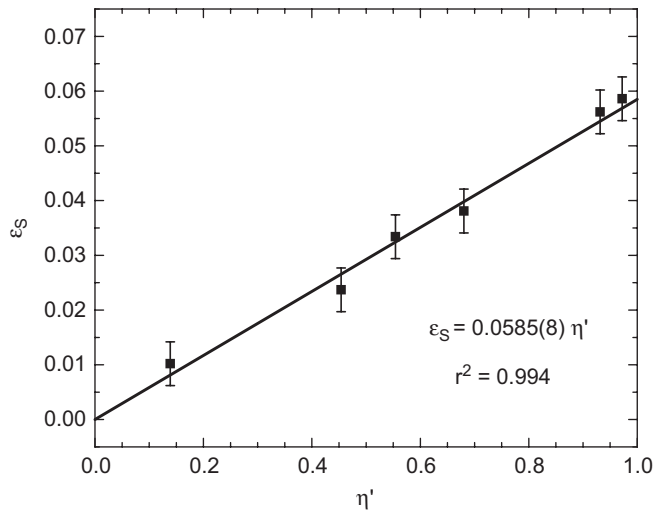

Fig. 9. Correlation between the spontaneous strain ε_s and the Landau order parameter η'. Squares: experimental data. Line: least-squares linear fit.

The deviation of the fergusonite structure from the $I4_1/a$ symmetry can be expressed by the magnitude of the order parameter η. According to the Landau theory [67] for a second-order transition, η is small and close to the critical value of the relevant thermodynamic variable (i.e. P_T). Under this hypothesis, the Gibbs free energy (G) of the fergusonite phase relative to the scheelite phase can be expressed as a Taylor expansion in terms of η yielding the following relation if only the first two terms are considered: $G = k_1(P - P_T)\eta^2 + k_2\eta^4$, where k_1 and k_2 are two constants [20]. As pressure drives the studied transition, from this equation, the relation between pressure and the order parameter can be found by minimizing G; i.e. when the condition $\partial G/\partial\eta = 0$ is satisfied. This condition is only fulfilled if the order parameter has the form: $\eta \propto \sqrt{(P - P_T)/P_T} = \eta'$, which can be defined as the phenomenological order parameter in Landau's theory [67]. In a ferroelastic transition ε_s can be considered as proportional to the primary order parameter η [70] and consequently also to η'. Therefore, if the pressure-induced scheelite to fergusonite phase transition is a second-order ferroelastic transition, ε_s should be a linear function in Fig. 9. In this figure, it can be seen that, within the uncertainty of the results, this condition is satisfied in $SrMoO_4$. Indeed, we found that $\varepsilon_s = 0.0585(8)\eta'$, with a correlation coefficient $r^2 = 0.994$. This fact strongly suggests that the scheelite to fergusonite transition studied here is a second-order phase transition. An analogous phase transition was obtained after analyzing the spontaneous strain in alkaline-earth orthotungstates [20] and in that case the proportionality constant was 20% smaller than in the present investigation. Further, a ferroelastic transition has been also found at low temperature in the isostructural scheelite $CaMoO_4$ [71]. In addition, the observation of a soft acoustic mode in Brillouin scattering measurements in scheelite-structured $BiVO_4$ [72] strongly supports our interpretation of the ferroelastic-type scheelite to fergusonite transition.

4. Conclusions

Our X-ray diffraction studies on strontium molybdate show that it transforms to the fergusonite phase around 12.2(9) GPa, as observed in isostructural barium molybdate [29] and strontium tungstate [17]. No additional phase transitions were observed up to 25 GPa and on release of pressure $SrMoO_4$ reverts back to the initial scheelite phase without any significant hysteresis. The high-pressure phase is a distorted and compressed version of scheelite obtained by a small distortion of the cation matrix and significant displacements of the anions. A mechanism for the transition is proposed and its characteristic features are discussed using the calculated spontaneous strain and the Landau theory. In particular, we found that the spontaneous strain is a linear function of the phenomenological order parameter defined in the Landau theory. This evidence strongly suggests that the studied pressure-induced phase transition is a second-order ferroelastic transformation. Finally a RT EOS for $SrMoO_4$ was determined with EOS parameters: $B_0 = 71(3)$ GPa, $B_0' = 4.2(4)$, and $V_0 = 349.7(4)$ Å^3. The compressibility of both the low- and high-pressure phases is highly anisotropic. This fact and the determined bulk compressibility are discussed in terms of the different compressibility of the SrO_8 and MoO_4 polyhedra.

Acknowledgments

This study was made possible through financial support from the Spanish government MCYT under Grants no. MAT2007-65990-C03-01 and CSD-2007-00045 and of the Nature Science Foundation of the Fujian Province of China under Grant no. 2005HZ1026. The US Department of Energy, Office of Science, and Office of Basic Energy Sciences supported the use of the APS under Contract no. W-31-109-Eng-38. DOE-BES, DOE-NNSA, NSF, DOD-TACOM, and the Keck Foundation supported the use of the HPCAT. D.E. acknowledges the financial support from the MCYT of Spain and the University of València through the "Ramón y Cajal" program. He is also indebted to the Fundación de las Artes y las Ciencias de Valencia for granting him the IDEA prize. Work at UNLV is supported by DOE award No. DEFG36-05GO08502. The UNLV High Pressure Science and Engineering Center is supported by the DOE-NNSA under cooperative agreement no. DE-FC52-06NA26274.

References

[1] A.W. Sleight, Acta Crystallogr. B 28 (1972) 2899.
[2] M. Ishii, M. Kobayashi, Prog. Cryst. Growth Charact. 23 (1991) 245.
[3] N. Faure, C. Borel, M. Couchaud, G. Basset, R. Templier, C. Wyon, Appl. Phys. B 63 (1996) 593.

[4] G. Angloher, C. Bucci, C. Cozzini, F. von Feilitzsch, T. Frank, D. Hauff, S. Henry, Th. Jagemann, J. Jochum, H. Kraus, B. Majorovits, J. Ninkovie, F. Petricca, F. Pröbst, Y. Ramachers, W. Rau, W. Seidel, M. Stark, S. Uchaikin, L. Stodolsky, H. Wulandari, Nucl. Instrum. Methods Phys. Res. A 520 (2004) 108.
[5] E.F. Paski, M.W. Blades, Anal. Chem. 60 (1988) 1224.
[6] M. Daturi, L. Savary, G. Costentin, J.C. Lavalley, Catal. Today 61 (2000) 231.
[7] N. Sharma, K.M. Shaju, G.V. Subba Rao, B.V.R. Chowdari, Z.L. Dong, T.J. White, Chem. Inform. 15 (2004) 101.
[8] A. Brenier, G.H. Jia, C.Y. Tu, J. Phys.: Condens. Matter 16 (2004) 9103.
[9] F.J. Manjón, D. Errandonea, N. Garro, J. Pellicer-Porres, P. Rodríguez-Hernández, S. Radescu, J. López-Solano, A. Mujica, A. Muñoz, Phys. Rev. B 74 (2006) 144111.
[10] F.J. Manjón, D. Errandonea, N. Garro, J. Pellicer-Porres, P. Rodríguez-Hernández, S. Radescu, J. López-Solano, A. Mujica, A. Muñoz, Phys. Rev. B 74 (2006) 144112.
[11] D. Errandonea, J. Pellicer-Porres, F.J. Manjón, A. Segura, Ch. Ferrer-Roca, R.S. Kumar, O. Tschauner, P. Rodríguez-Hernández, J. López-Solano, S. Radescu, A. Mujica, A. Muñoz, G. Aquilanti, Phys. Rev. B 72 (2005) 174106.
[12] D. Errandonea, J. Pellicer-Porres, F.J. Manjón, A. Segura, Ch. Ferrer-Roca, R.S. Kumar, O. Tschauner, J. López-Solano, P. Rodríguez-Hernández, S. Radescu, A. Mujica, A. Muñoz, G. Aquilanti, Phys. Rev. B 73 (2006) 224103.
[13] D. Christofilos, K. Papagelis, S. Ves, G.A. Kourouklis, C. Raptis, J. Phys.: Condens. Matter 14 (2002) 12641.
[14] D. Christofilos, S. Ves, G.A. Kourouklis, Phys. Status Solidi B 198 (1996) 539.
[15] V. Panchal, N. Garg, A.K. Chauhan, Sangeeta, S.M. Sharma, Solid State Commun. 130 (2004) 203.
[16] D. Errandonea, M. Somayazulu, D. Häusermann, Phys. Status Solidi B 235 (2003) 162.
[17] D. Errandonea, M. Somayazulu, D. Häusermann, Phys. Status Solidi B 231 (2002) R1.
[18] D. Christofilos, E. Efthimiopoulos, J. Arvanitidis, K. Papagelis, S. Ves, G.A. Kourouklis, High Pressure Res. 26 (2006) 421.
[19] D. Errandonea, Phys. Status Solidi B 242 (2005) R125.
[20] D. Errandonea, Europhys. Lett. 77 (2007) 56001.
[21] D. Errandonea, D. Martínez-García, R. Lacomba-Perales, J. Ruiz-Fuertes, A. Segura, Appl. Phys. Lett. 89 (2006) 091913.
[22] D. Errandonea, C.Y. Tu, G.H. Jia, I.R. Martın, U.R. Rodrıguez-Mendoza, F. Lahoz, M.E. Torres, V. Lavın, J. Alloys Compds. 452 (2008).
[23] D. Christofilos, J. Arvanitidis, E. Kampesekali, K. Papagelis, S. Ves, G.A. Kourouklis, Phys. Status Solidi B 241 (2004) 3155.
[24] A. Jayaraman, B. Batlogg, L.G. VanUitert, Phys. Rev. B 31 (1985) 5423.
[25] A. Jayaraman, S.Y. Wang, S.R. Shieh, S.K. Sharma, L.C. Ming, J. Raman Spectrosc. 26 (1995) 451.
[26] E. Sarantopoulou, C. Raptis, S. Ves, D. Christofilos, G.A. Kourouklis, J. Phys.: Condens. Matter 14 (2002) 8925.
[27] A. Jayaraman, S.W. Wang, S.K. Sharma, Phys. Rev. B 52 (1995) 9886.
[28] W.A. Crichton, A. Grzechnik, Z. Kristallogr. 219 (2004) 337.
[29] V. Panchal, N. Garg, S.M. Sharma, J. Phys.: Condens. Matter 18 (2006) 3917.
[30] S.R. Shieh, L.C. Ming, A. Jayaraman, J. Phys. Chem. Solids 57 (1996) 205.
[31] J. Lopez-Solano, P. Rodriguez-Hernandez, S. Radescu, A. Mujica, A. Muñoz A., D. Errandonea, F.J. Manjon, J. Pellicer-Porres, N. Garro, A. Segura, Ch. Ferrer-Roca, R.S. Kumar, O. Tschauner, G. Aquilanti, Phys. Status Solidi B 244 (2007) 325.
[32] G.H. Jia, C.Y. Tu, Z.Y. You, J.F. Li, Z.J. Zhu, Y. Wang, B.C. Wu, J. Cryst. Growth 273 (2004) 220.
[33] E. Gurmen, E. Daniels, J.S. King, J. Chem. Phys. 55 (1971) 1093.
[34] H.K. Mao, J. Xu, P.M. Bell, J. Geophys. Res. 91 (1986) 4673.
[35] Y. Shen, R.S. Kumar, M. Pravica, M.F. Nicol, Rev. Sci. Instrum. 75 (2004) 4450.
[36] D. Errandonea, Y. Meng, M. Somayazulu, D. Häusermann, Physica B 355 (2005) 116.
[37] A.P. Hammersley, S.O. Svensson, M. Hanfland, A.N. Fitch, D. Häusermann, High Pressure Res. 14 (1996) 235.
[38] W. Kraus, G. Nolze, J. Appl. Crystallogr. 301 (1996) 29.
[39] D. Errandonea, F.J. Manjón, M. Somayazulu, D. Häusermann, J. Solid State Chem. 177 (2004) 1087.
[40] F. Birch, J. Geophys. Res. 83 (1978) 1257.
[41] R.M. Hazen, L.W. Finger, J.W.E. Mariathasan, J. Phys. Chem. Solids 46 (1985) 253.
[42] V.T. Deshpande, S.V. Suryanarayana, Acta Crystallogr. A 28 (1972) 94.
[43] S.N. Achary, S.J. Patwe, M.D. Mathews, A.K. Tyagi, J. Phys. Chem. Solids 67 (2006) 774.
[44] J.W.E. Mariathasan, L.W. Finger, R.M. Hazen, Acta Crystallogr. B 41 (1984) 179.
[45] A.I. Komkov, Mem. All-Union Min. Soc. 86 (1957) 432.
[46] F.J. Manjón, D. Errandonea, J. López-Solano, P. Rodríguez-Hernández, S. Radescu, A. Mujica, A. Muñoz, N. Garro, J. Pellicer-Porres, A. Segura, Ch. Ferrer-Roca, R.S. Kumar, O. Tschauner, G. Aquilanti, Phys. Status Solidi B 244 (2007) 295.
[47] J.P. Bastide, J. Solid State Chem. 71 (1987) 115.
[48] D. Errandonea, R. Boehler, M. Ross, Phys. Rev. B 65 (2002) 012108.
[49] H.L. Skriver, Phys. Rev. B 31 (1985) 1909.
[50] C. Keller, Zeitschrift für Anorganische und Allgemeine Chemie 318 (2004) 89.
[51] L.E. Depero, L. Sangaletti, J. Solid State Chem. 129 (1997) 82.
[52] I. Kawada, K. Kato, T. Fujita, Acta Crystallogr. 30 (1974) 2069.
[53] W. Jeitschko, A.W. Sleight, Acta Crystallogr. 29 (1973) 869.
[54] T. Fujita, I. Kawada, K. Kato, Acta Crystallogr. 33 (1977) 162.
[55] M. Daturi, M.M. Borel, A. Leclaire, L. Savary, G. Costentin, J.C. Lavalley, B. Raveau, J. Chem. Phys. 93 (1996) 2043.
[56] Y.A. Titov, A.M. Sych, A.N. Sokolov, A.A. Kapshuk, V. Ya Markiv, N.M. Belyavina, J. Alloys Compds. 311 (2000) 252.
[57] E.T. Keve, S.C. Abrahams, J.L. Bernstein, J. Chem. Phys. 51 (1969) 4928.
[58] B.O. Loopstra, H.M. Rietveld, Acta Crystallogr. 25 (1969) 787.
[59] R.W.G. Wyckoff, Z. Kristallogr. 66 (1927) 73.
[60] J. Beintema, Z. Kristallogr. 97 (1937) 300.
[61] D. Errandonea, J. Phys. Chem. Solids 67 (2006) 2017.
[62] A. Grzechnik, W.A. Crichton, M. Hanfland, Phys. Status Solidi B 242 (2005) 2795.
[63] D. Errandonea, R. Boehler, S. Japel, M. Mezouar, L.R. Benedetti, Phys. Rev. B 73 (2006) 092106.
[64] D. Errandonea, B. Schwager, R. Boehler, M. Ross, Phys. Rev. B 65 (2002) 214110.
[65] C.S. Yoo, H. Cynn, P. Soderlind, V. Iota, Phys. Rev. Lett. 84 (2000) 4132.
[66] L. Jian, C.M. Wayman, J. Am. Ceram. Soc. 80 (1997) 803.
[67] L.D. Landau, E.M. Lifshitz, Statistical Physics Part I, in: Course of Theoretical Physics, vol. 5, third ed. Pergamon Press, Oxford, 1994.
[68] J.L. Schlenker, G.V. Gibbs, M.B. Boisen, Acta Crystallogr. A 34 (1978) 52.
[69] K. Aizu, J. Phys. Soc. Jpn. 28 (1970) 706.
[70] J. Haines, J.M. Léger, Phys. Rev. B 48 (1993) 13344.
[71] J. Simon, J. Banys, J. Hoentsch, G. Völkel, R. Böttcher, A. Hofstaetter, A. Scharmann, J. Phys. Condens. Matter 8 (1996) L359.
[72] G. Benyuan, M. Copic, H.Z. Cummins, Phys. Rev. B 24 (1981) 4098.